Biomedical Optics EXPRESS

Three-dimensional transillumination image reconstruction for small animal with new scattering suppression technique

Trung Nghia Tran,[1,*] Kohei Yamamoto,[1] Takeshi Namita,[1,2] Yuji Kato,[1] and Koichi Shimizu[1]

[1]*Graduate School of Information Science and Technology, Hokkaido University, North 14 West 9, Kita-ku, Sapporo 060-0814, Japan*

[2]*Currently with the Graduate School of Medicine, Kyoto University, 53 Shogoin Kawahara-cho, Sakyo-ku, Kyoto 606-8507, Japan*

[*]*tran@bme.ist.hokudai.ac.jp*

Abstract: To realize three-dimensional (3D) optical imaging of the internal structure of an animal body, we have developed a new technique to reconstruct optical computed tomography (optical CT) images from two-dimensional (2D) transillumination images. In transillumination imaging of an animal body using near-infrared light, the image is blurred because of the strong scattering in the tissue. To overcome this problem, we propose a novel technique to apply the point spread function (PSF) for a light source located inside the medium to the transilluminated image of light-absorbing structure. The problem of the depth-dependence of PSF was solved in the calculation of the projection image in the filtered back-projection method. The effectiveness of the proposed technique was assessed in the experiments with a model phantom and a mouse. These analyses verified the feasibility of the practical 3D imaging of the internal light-absorbing structure of a small animal.

OCIS codes: (100.1830) Deconvolution; (170.3010) Image reconstruction techniques; (170.3880) Medical and biological imaging; (170.6960) Tomography; (170.7050) Turbid media.

References and links

1. R. Bright, *Diseases of the brain and nervous system vol. II* (London: Longman, 1831).
2. T. B. Curling, *A practical treatise on the diseases of the testis and of the spermatic cord and scrotum* (London: Samuel Highley, 1843).
3. M. Cutler, "Transillumination as an aid in the diagnosis of breast lesions," Surg. Gynecol. Obstet. **48**, 721–728 (1929).
4. J. C. Hebden, S. R. Arridge, and D. T. Delpy, "Optical imaging in medicine: I. Experimental techniques," Phys. Med. Biol. **42**(5), 825–840 (1997).
5. R. Weissleder and V. Ntziachristos, "Shedding light onto live molecular targets," Nat. Med. **9**(1), 123–128 (2003).
6. A. H. Hielscher, "Optical tomographic imaging of small animals," Curr. Opin. Biotechnol. **16**(1), 79–88 (2005).
7. A. P. Gibson, J. C. Hebden, and S. R. Arridge, "Recent advances in diffuse optical imaging," Phys. Med. Biol. **50**(4), R1–R43 (2005).
8. V. Ntziachristos, "Fluorescence molecular imaging," Annu. Rev. Biomed. Eng. **8**(1), 1–33 (2006).
9. A. Gibson and H. Dehghani, "Diffuse optical imaging," Philos Trans A Math Phys Eng Sci **367**(1900), 3055–3072 (2009).
10. F. Leblond, S. C. Davis, P. A. Valdés, and B. W. Pogue, "Pre-clinical whole-body fluorescence imaging: Review of instruments, methods and applications," J. Photochem. Photobiol. B **98**(1), 77–94 (2010).
11. B. D'Alessandro and A. P. Dhawan, "Transillumination imaging for blood oxygen saturation estimation of skin lesions," IEEE Trans. Biomed. Eng. **59**(9), 2660–2667 (2012).
12. J. A. Guggenheim, H. R. A. Basevi, J. Frampton, I. B. Styles, and H. Dehghani, "Multi-modal molecular diffuse optical tomography system for small animal imaging," Meas. Sci. Technol. **24**(10), 105405 (2013).
13. F. F. Jöbsis, "Noninvasive, infrared monitoring of cerebral and myocardial oxygen sufficiency and circulatory parameters," Science **198**(4323), 1264–1267 (1977).
14. M. Cope and D. T. Delpy, "System for long-term measurement of cerebral blood and tissue oxygenation on newborn infants by near infra-red transillumination," Med. Biol. Eng. Comput. **26**(3), 289–294 (1988).

#205296 - $15.00 USD Received 23 Jan 2014; revised 6 Mar 2014; accepted 7 Mar 2014; published 1 Apr 2014

15. G. Gratton, P. M. Corballis, E. Cho, M. Fabiani, and D. C. Hood, "Shades of gray matter: noninvasive optical images of human brain responses during visual stimulation," Psychophysiology **32**(5), 505–509 (1995).
16. E. Okada, M. Firbank, M. Schweiger, S. R. Arridge, M. Cope, and D. T. Delpy, "Theoretical and experimental investigation of near-infrared light propagation in a model of the adult head," Appl. Opt. **36**(1), 21–31 (1997).
17. F. F. Jobsis-Vandervliet, "Discovery of the near-infrared window into the body and the early development of near-infrared spectroscopy," J. Biomed. Opt. **4**(4), 392–396 (1999).
18. Y. Taka, Y. Kato, and K. Shimizu, "Transillumination imaging of physiological functions by NIR light," in Proceedings of IEEE Conference on 22nd Annual International Conference of the IEEE Engineering in Medicine and Biology Society (IEEE, 2000), pp. 771–774.
19. H. Obrig and A. Villringer, "Beyond the visible--imaging the human brain with light," J. Cereb. Blood Flow Metab. **23**(1), 1–18 (2003).
20. Y. Hoshi, "Functional near-infrared optical imaging: utility and limitations in human brain mapping," Psychophysiology **40**(4), 511–520 (2003).
21. I. Nishidate, Y. Aizu, and H. Mishina, "Depth visualization of a local blood region in skin tissue by use of diffuse reflectance images," Opt. Lett. **30**(16), 2128–2130 (2005).
22. M. Wolf, M. Ferrari, and V. Quaresima, "Progress of near-infrared spectroscopy and topography for brain and muscle clinical applications," J. Biomed. Opt. **12**(6), 062104 (2007).
23. T. Hamaoka, K. K. McCully, V. Quaresima, K. Yamamoto, and B. Chance, "Near-infrared spectroscopy/imaging for monitoring muscle oxygenation and oxidative metabolism in healthy and diseased humans," J. Biomed. Opt. **12**(6), 062105 (2007).
24. A. Y. Bluestone, G. Abdoulaev, C. Schmitz, R. L. Barbour, and A. H. Hielscher, "Three-dimensional optical tomography of hemodynamics in the human head," Opt. Express **9**(6), 272–286 (2001).
25. D. A. Boas, D. H. Brooks, E. L. Miller, C. A. DiMarzio, M. Kilmer, R. J. Gaudette, and Q. Zhang, "Imaging the body with diffuse optical tomography," IEEE Signal Process. Mag. **18**(6), 57–75 (2001).
26. H. Jiang, Y. Xu, N. Iftimia, J. Eggert, K. Klove, L. Baron, and L. Fajardo, "Three-dimensional optical tomographic imaging of breast in a human subject," IEEE Trans. Med. Imaging **20**(12), 1334–1340 (2001).
27. A. H. Hielscher, A. Y. Bluestone, G. S. Abdoulaev, A. D. Klose, J. Lasker, M. Stewart, U. Netz, and J. Beuthan, "Near-infrared diffuse optical tomography," Dis. Markers **18**(5-6), 313–337 (2002).
28. F. Gao, H. Zhao, and Y. Yamada, "Improvement of image quality in diffuse optical tomography by use of full time-resolved data," Appl. Opt. **41**(4), 778–791 (2002).
29. J. C. Hebden, A. Gibson, R. M. Yusof, N. Everdell, E. M. C. Hillman, D. T. Delpy, S. R. Arridge, T. Austin, J. H. Meek, and J. S. Wyatt, "Three-dimensional optical tomography of the premature infant brain," Phys. Med. Biol. **47**(23), 4155–4166 (2002).
30. H. Dehghani, B. W. Pogue, S. P. Poplack, and K. D. Paulsen, "Multiwavelength three-dimensional near-infrared tomography of the breast: initial simulation, phantom, and clinical results," Appl. Opt. **42**(1), 135–145 (2003).
31. J. P. Culver, A. M. Siegel, J. J. Stott, and D. A. Boas, "Volumetric diffuse optical tomography of brain activity," Opt. Lett. **28**(21), 2061–2063 (2003).
32. D. A. Boas, K. Chen, D. Grebert, and M. A. Franceschini, "Improving the diffuse optical imaging spatial resolution of the cerebral hemodynamic response to brain activation in humans," Opt. Lett. **29**(13), 1506–1508 (2004).
33. B. W. Pogue, S. C. Davis, X. Song, B. A. Brooksby, H. Dehghani, and K. D. Paulsen, "Image analysis methods for diffuse optical tomography," J. Biomed. Opt. **11**(3), 033001 (2006).
34. L. C. Enfield, A. P. Gibson, N. L. Everdell, D. T. Delpy, M. Schweiger, S. R. Arridge, C. Richardson, M. Keshtgar, M. Douek, and J. C. Hebden, "Three-dimensional time-resolved optical mammography of the uncompressed breast," Appl. Opt. **46**(17), 3628–3638 (2007).
35. K. Shimizu, K. Tochio, and Y. Kato, "Improvement of transcutaneous fluorescent images with a depth-dependent point-spread function," Appl. Opt. **44**(11), 2154–2161 (2005).
36. D. S. C. Biggs and M. Andrews, "Acceleration of iterative image restoration algorithms," Appl. Opt. **36**(8), 1766–1775 (1997).
37. R. J. Hanisch, R. L. White, and R. L. Gilliland, "Deconvolution of hubble space telescope images and spectra," in *Deconvolution of Images and Spectra*, P.A. Jansson, ed. (Academic Press, Boston, MA, 1997).
38. Science Council of Japan, *Guidelines for proper conduct of animal experiments* (2006).

1. Introduction

Three-dimensional imaging with X-ray or MRI has contributed greatly not only to medical diagnosis, but also to life science. The number of experimental animals killed for experimentation would be reduced if we were able to visualize the animals' internal structures non-invasively. In transillumination imaging using near-infrared (NIR) light, we can visualize the location of internal bleeding, infection, and angiogenesis [1–12]. Functional imaging is also possible using spectroscopic principles [4–23]. With specific contrast media, the usefulness of NIR imaging is expanded significantly.

The possibility and the potential of the NIR transillumination technique were pointed out early [1–3], but the technique has not been used widely. The major reason for that relative lack of use is the difficulty of the strong scattering in tissues [1–12]. In transillumination

#205296 - $15.00 USD Received 23 Jan 2014; revised 6 Mar 2014; accepted 7 Mar 2014; published 1 Apr 2014

images, the deeper structure is blurred and cannot be differentiated from the shallower and less-absorbing structure. To overcome this problem, great effort has been undertaken to develop optical computed tomography (optical CT) techniques. The typical technique for a macroscopic structure is diffuse optical tomography (DOT) [24–34]. Using this technique, cross-sectional imaging of human breasts and infant heads was achieved. Once the cross-sectional images become available, 3D imaging is possible. However, current techniques require great computational effort such as finite element method calculation, and large devices such as numerous fiber bundles around the object body.

We would be able to reconstruct the 3D structure with a common filtered back-projection algorithm and with a CCD or CMOS camera if we were able to suppress the scattering effect in transillumination images effectively. They require much simpler and more compact device as well as much less computational effort.

For scattering suppression, the deconvolution technique using the point spread function (PSF) is effective. We have derived the PSF for the fluorescent light source by applying the diffusion approximation to the equation of transfer [35]. With the known depth of the light source in a diffuse medium, we can recover the fluorescent distribution clearly through an interstitial tissue by the deconvolution with this PSF. Therefore, we could expect to realize the 3D imaging from the transillumination images if we were able to apply this light-source PSF to the absorbing structure and thereby solve the problem of the depth-dependence of the PSF.

In this paper, we propose the 3D imaging of internal absorbing structure of a small experimental animal from 2D NIR transillumination images using new scatter-suppression techniques.

2. Scattering suppression by PSF deconvolution

For the fluorescent point source at depth d as shown in Fig. 1, the PSF is given as [35],

$$PSF(\rho)=\frac{3P_0}{(4\pi)^2}\left\{(\mu'_s+\mu_a)+\left[\kappa_d+\frac{1}{(\rho^2+d^2)^{1/2}}\right]\frac{d}{(\rho^2+d^2)^{1/2}}\right\}\frac{\exp\left[-\kappa_d(\rho^2+d^2)^{1/2}\right]}{(\rho^2+d^2)^{1/2}}, \quad (1)$$

where P_0, μ'_s, μ_a, d, and ρ respectively stand for the optical power of a point source, the reduced scattering coefficient, the absorption coefficient, the depth of a point source, and the radial distance in the cylindrical coordinate system. $\kappa_d=\sqrt{3\mu_a(\mu'_s+\mu_a)}$.

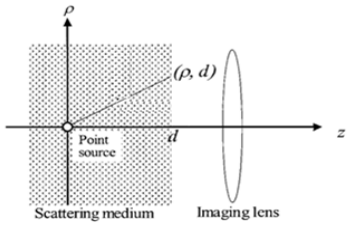

Fig. 1. Geometry for PSF as light distribution observed at the scattering medium surface.

This PSF was obtained as the light image from a point light source observed at the scattering medium surface. Therefore, its applicability to the transillumination image of an absorbing structure must be examined. In transillumination imaging, homogeneous light is irradiated from outside of the scattering medium. The scattered light goes through the absorbing structure and projects the shadow on the surface of the scattering medium. We can consider the absorber as a collection of light-missing points if the light is diffused well at the depth of the absorbing structure. Then the absorber image observed at the surface is the collection of the spread light-missing distributions which are the PSFs obtained above. We can apply the Eq. (1) to the transillumination image of an absorbing structure if this assumption is correct.

#205296 - $15.00 USD Received 23 Jan 2014; revised 6 Mar 2014; accepted 7 Mar 2014; published 1 Apr 2014

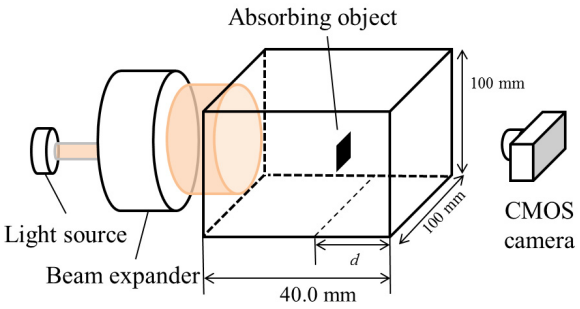

Fig. 2. Experimental setup for transillumination imaging: d = 4.00–14.0 mm.

The applicability described above was assessed in an experiment. Figure 2 shows the experimental system. As a scattering medium, an Intralipid suspension (Fresenius Kabi AG) was mixed with distilled water and black ink (INK-30-B; Pilot Corp.) to produce a tissue-equivalent medium (μ'_s = 1.00 /mm, μ_a = 0.01 /mm). As an absorbing structure, a square black-painted metal plate (10.0 × 10.0 × 1.00 mm^3) was used. This absorber was placed in an acrylic container (40.0 × 100 × 100 mm^3) filled with scattering medium. The depth of the absorber from the observation surface was variable from 4.00 to 14.0 mm. This phantom was irradiated with the NIR light from a laser (Ti:Sapphire, 800 nm wavelength) through a beam expander for homogeneous illumination. An image is obtained using a cooled CMOS camera (C11440-10C; Hamamatsu Photonics K.K.) oriented toward the opposite face of the phantom to the light-incident side.

We first obtained a transillumination image $f_o(x, y)$ of an absorbing object in a transparent medium, or clear water. Subsequently, we replaced the water with the scattering medium, and obtained the transillumination image $f_s(x, y)$. The measured PSF for the absorbing structure $PSF_{abs}(x, y)$ was calculated as

$$PSF_{abs}(x, y) = f_s(x, y) \otimes f_o(x, y), \tag{2}$$

where $\otimes$ denotes the deconvolution operation.

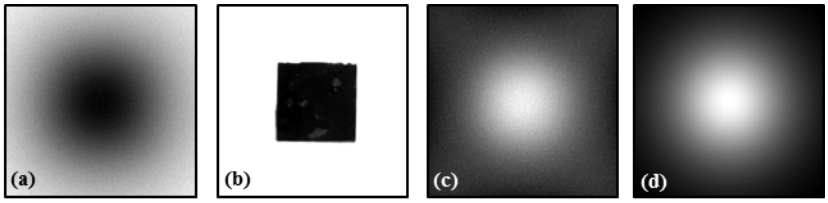

Fig. 3. Comparison of point spread function at depth d = 8.00 mm: (a) $f_s(x, y)$, (b) $f_o(x, y)$, (c) $PSF_{abs}(x, y)$ from Eq. (2), (d) PSF from Eq. (1).

The measured $PSF_{abs}(x, y)$ was compared with the theoretical PSF of the fluorescent source or Eq. (1) using the same conditions as those of the experiment. Figure 3 shows the comparison of PSF at depth d = 8.00 mm. Figures 3(a), 3(b), 3(c), and 3(d) respectively show the observed transillumination image with the scattering medium $f_s(x, y)$, with the transparent medium $f_o(x, y)$, measured PSF for absorbing structure $PSF_{abs}(x, y)$ calculated from Eq. (2), and PSF calculated from Eq. (1). Figures 3(c) and 3(d) show good agreement between the PSF_{abs} from Eq. (2) and the PSF from Eq. (1). Figure 4 shows the result of the comparison in terms of the spread (FWHM) of these two PSFs. At the same depth d, both PSFs were in good agreement.

Through this analysis, it was confirmed that the depth-dependent PSF for the fluorescent light source is applicable to the transillumination images of the absorbing structure.

#205296 - $15.00 USD Received 23 Jan 2014; revised 6 Mar 2014; accepted 7 Mar 2014; published 1 Apr 2014

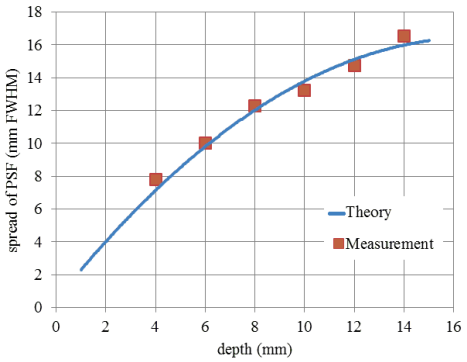

Fig. 4. Comparison between theoretical PSF for light source and measured PSF for absorber.

Experimental verification of scattering suppression

The effectiveness of the PSF from Eq. (1) to suppress the scattering effect in a transillumination image of the absorbing structure was examined in another experiment. In the deconvolution process, the Lucy–Richardson algorithm [36,37] with iteration number up to 10 was used.

A Y-shaped black tube (4.00 mm diameter) was placed at 4.00 mm depth from the observation surface. Figure 5(a) shows the image through clear water. Figures 5(b) and 5(c) respectively show the observed transillumination image and the result of deconvolution with the PSF at 4.00 mm depth. The separation of Y-shaped arms was clarified by the deconvolution with an appropriate PSF. The effectiveness is apparent in the intensity profiles shown in Fig. 6 as well. The average Michelson contrasts were, respectively, 0.31 and 0.77 for observed and deconvoluted images. The sharpness parameters of these images were respectively, 0.18 and 0.54 for observed and deconvoluted images.

Through this experimental analysis, it was confirmed that the PSF derived for a fluorescent light source is applicable and effective to suppress the scattering effect in transillumination images.

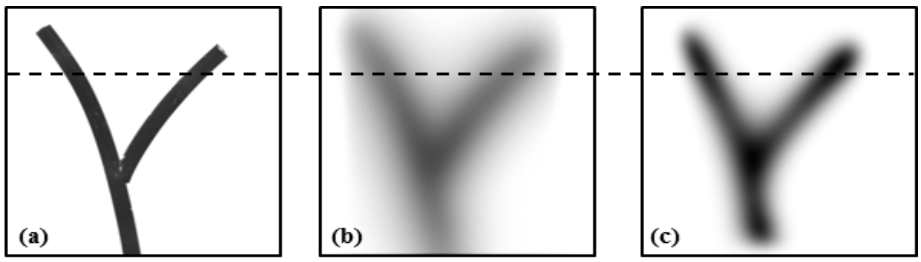

Fig. 5. Transillumination image: (a) original object, (b) observed image, (c) deconvoluted image.

#205296 - $15.00 USD Received 23 Jan 2014; revised 6 Mar 2014; accepted 7 Mar 2014; published 1 Apr 2014

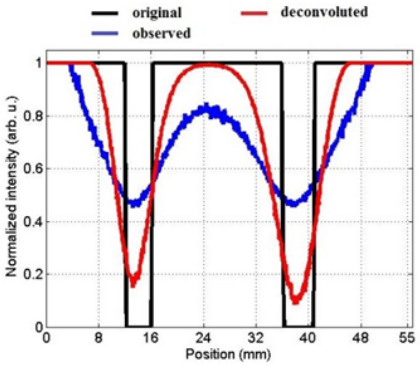

Fig. 6. Intensity profiles along the dashed line in Fig. 5.

3. 3D reconstruction from transillumination images

3.1 Tissue-equivalent phantom

Considering a transillumination image as a projection in the computed tomography, one can reconstruct the 3D structure of the internal absorption distribution of a turbid medium. The feasibility of this 3D reconstruction was examined in an experiment. Figures 7 and 8 show the experimental setup and the target structure of this experiment. A slant cylindrical post (3.00 mm diameter, 30.6 mm length) was fixed in the acrylic container (35.0 × 100 × 100 mm^3) filled with a scattering medium. Intralipid suspension (Fresenius Kabi AG) was mixed with distilled water to produce tissue-equivalent medium (μ'_s = 1.00 /mm, μ_a = 0.00536 /mm). Laser light (Ti:Sapphire, 850 nm wavelength) was illuminated from one side of the container and the transillumination image was recorded using a cooled CMOS camera (C11440-10C; Hamamatsu Photonics K.K.) from another side of the container. This recording was repeated while rotating the absorber post around the rotation axis shown in Fig. 8 using a mechanical rotary motion system.

In this case, the depth of the absorber from the observing surface of the scattering medium was not constant along the vertical axis of rotation. Therefore, the PSFs with known different depths were applied to a transillumination image, and horizontal intensity profiles were extracted at the proper vertical heights in the improved image obtained by the proper PSF with the correct depth. These horizontal intensity profiles were obtained from different circumferential orientations. The cross-sectional image was reconstructed using the filtered back-projection algorithm. Finally, we piled up the cross-sectional images along the vertical axis and reconstructed the 3D structure.

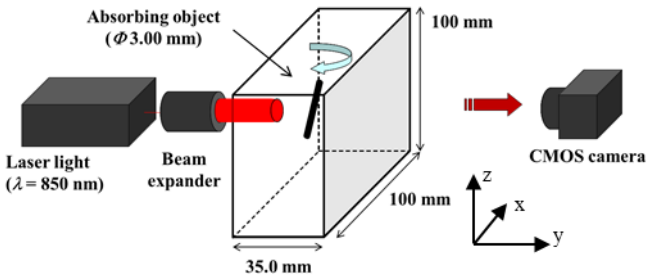

Fig. 7. Experimental setup.

#205296 - $15.00 USD Received 23 Jan 2014; revised 6 Mar 2014; accepted 7 Mar 2014; published 1 Apr 2014

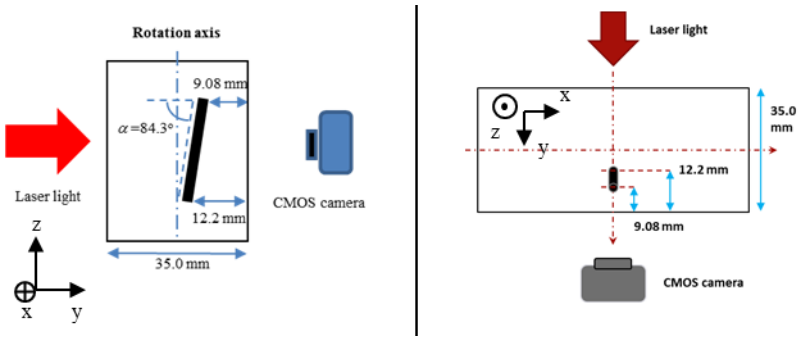

Fig. 8. Side view and top view of phantom model.

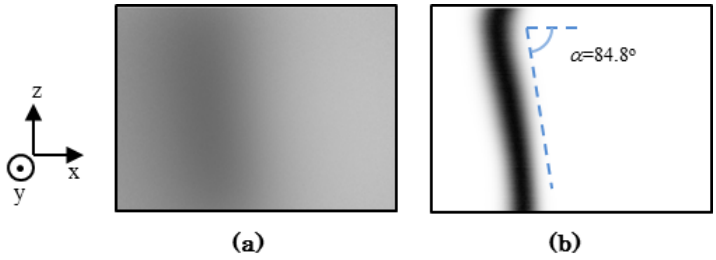

Fig. 9. Observed and deconvoluted images of absorber: (a) observed image (contrast and sharpness are 0.10 and 0.020), (b) deconvoluted image (contrast and sharpness are 0.90 and 0.71).

Figure 9 shows the observed transillumination image and the result of the PSF deconvolution. In this case, the absorbing post was parallel to the observation surface, and we were able to use the PSF with a single depth. The observed image was degraded severely by the effect of strong scattering. Its effect was greatly suppressed when using the proposed technique. Figures 10 and 11 show the cross-sectional images reconstructed from the observed and deconvoluted transillumination images. With the observed images, the position of the absorber was difficult to identify in cross-sectional images. They became clearly identifiable using the proposed technique. We analyzed the accuracy of the cross-sectional image at 10 different heights. The reconstruction error in the estimated depth $\hat{d}$ in the improved cross-sectional images varied 0.25–2.97% along the vertical axis.

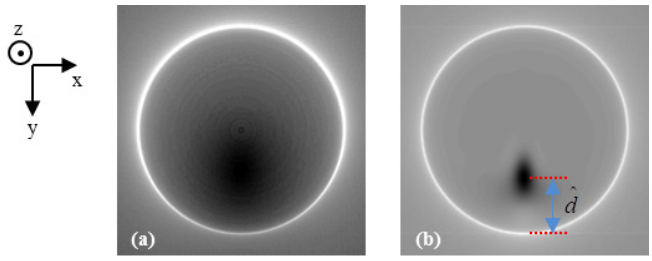

Fig. 10. CT image at the top of the absorber: (a) from observed images, (b) from deconvoluted images. Depth of estimated absorber center ($\hat{d}$) was 9.35 mm for true depth 9.08 mm.

#205296 - $15.00 USD Received 23 Jan 2014; revised 6 Mar 2014; accepted 7 Mar 2014; published 1 Apr 2014

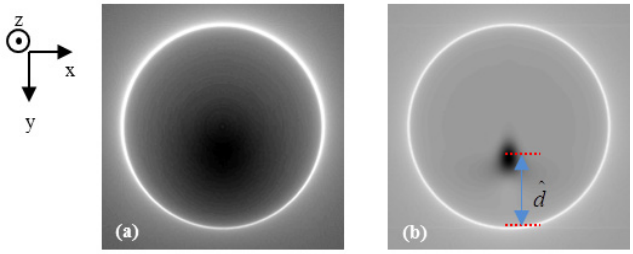

Fig. 11. CT image at the bottom of the absorber: (a) from observed images, (b) from deconvoluted images. Depth of estimated absorber center ($\hat{d}$) was 12.1 mm for true depth 12.2 mm.

Figure 12 shows the result of the 3D reconstruction. The absorbing structure in tissue-equivalent medium was reconstructed clearly using the proposed technique.

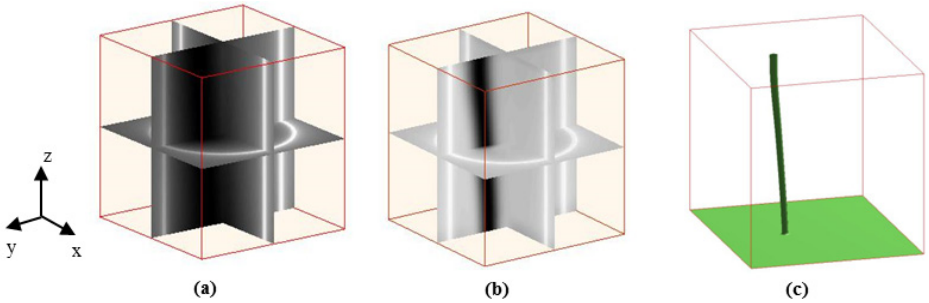

Fig. 12. 3D Reconstruction of absorber in turbid medium: (a) from observed images, (b) from deconvoluted images, (c) result of thresholding on image (b) with a single threshold value.

3.2 Animal-tissue phantom

To validate the accuracy of the result in heterogeneous animal tissue, 3D imaging was attempted with known absorbing structure. The method of the experiment was the same as that with the tissue-equivalent phantom mentioned above. A black-painted slant cylindrical post (3.00 mm diameter, 30.1 mm length) was fixed in the rectangular container filled with chicken breast meat. A transparent acrylic cylindrical tube (30.0 mm diameter, 2.00 mm wall thickness) rotated the post around the rotation axis.

Figure 13 shows an example of the transillumination image at 0 degree and the result of the proposed technique. The scattering effect was suppressed efficiently, and the absorbing objects were visualized. The center of the absorber was estimated in the cross-sectional images at 10 different heights. The estimation errors of the center varied 1.35–2.72% along the vertical axis. Figure 14 shows the result of 3D reconstruction. Using the proposed technique, the absorbing structure was reconstructed clearly in the heterogeneous animal tissue, as well.

#205296 - $15.00 USD Received 23 Jan 2014; revised 6 Mar 2014; accepted 7 Mar 2014; published 1 Apr 2014

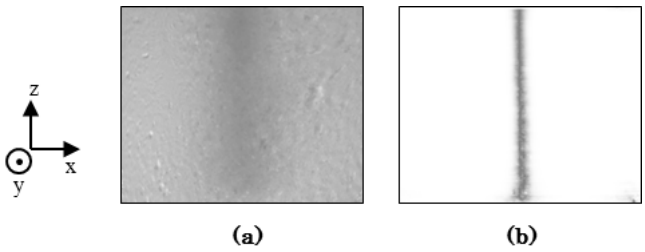

Fig. 13. Observed and deconvoluted images of absorber at 0-deg orientation: (a) observed image (b) result using the proposed technique.

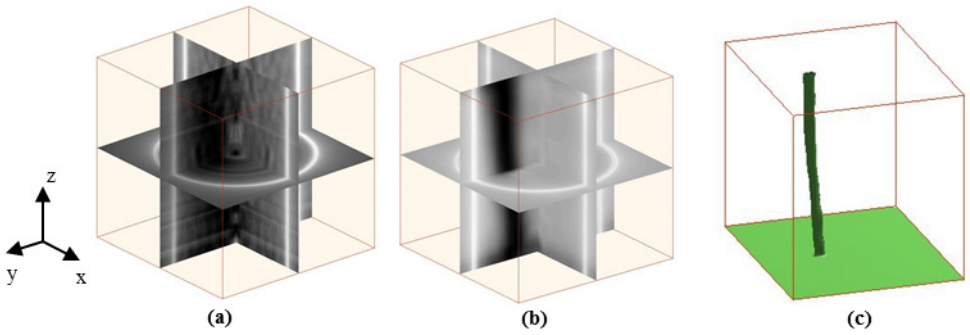

Fig. 14. 3D Reconstruction of absorber in animal tissue: (a) from observed images, (b) from deconvoluted images, (c) result of thresholding on image (b) with a single threshold value.

4. Application of depth-dependent PSF for unknown structure

As shown in the previous chapter, we can suppress the scattering effect in transillumination images and reconstruct the structure in a turbid medium. The blurring effect of scattering can be suppressed effectively by deconvolution with the depth-dependent PSF (Eq. (1)). Therefore, this technique is powerful when examining a known discrete structure such as that described in the preceding chapter. However, the structure is often unknown and not as simple as described above. The transillumination image is the integration of all the absorbing distribution in different depths with different blurring. Therefore, the scattering suppression with the PSF at a single depth is not effective for such a case. The usefulness of the proposed method would be expanded greatly if we were able to apply this technique to the object with unknown structure.

To overcome this problem, we developed a new technique to reconstruct a 3D structure from the blurred transillumination images using the depth-dependent PSF. Figure 15 shows the condition of a transillumination image of two absorbing objects at different depth in a turbid medium. The observed image appears as shown in Fig. 15(b). The absorption profile in the observed intensity is shown in the lower part of Fig. 15(b). The developed technique consists of two processes. The first process is the deconvolution of a transillumination image with the PSFs at varying depths. Figure 16 presents this process. The principle is shown in one dimension for simplicity instead of two dimension. All the deconvoluted data are summed to produce the projection data for the filtered back-projection process in the optical CT reconstruction. In this way, the true profile of the absorbing object is included in the projection data. In practice, two-dimensional PSFs at different depths are applied to a 2D transillumination image. The deconvoluted images are summed up to produce a projection image for 3D-optical CT reconstruction.

#205296 - $15.00 USD Received 23 Jan 2014; revised 6 Mar 2014; accepted 7 Mar 2014; published 1 Apr 2014

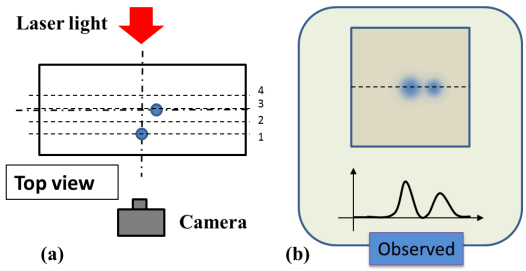

Fig. 15. Two absorbing objects in turbid medium: (a) top view of observing condition, (b) observed transillumination image and absorption profile along the dashed line.

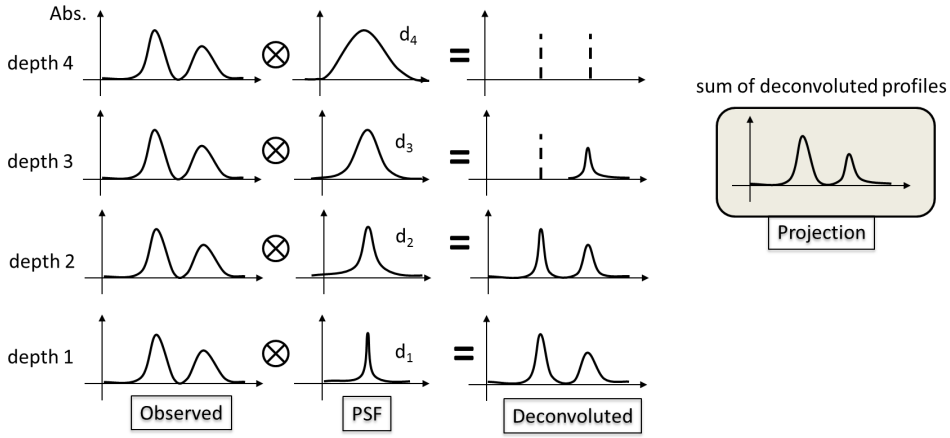

Fig. 16. Absorption profiles before and after the deconvolution with PSFs at different depths. The projection is obtained as a sum of the deconvoluted data with the PSFs at different depths. Profile of projection for cross-sectional reconstruction is shown in upper right corner. ⊗ denotes the deconvolution operation.

This process can be written as

$$P(x,z\,|\,\theta)=\sum_{i=1}^{n}\int A(x,y,z\,|\,\theta)dy\otimes PSF(x,z\,|\,d_i), \tag{3}$$

where P, A, and PSF respectively represent the functions of projection, blurred absorption distribution and point spread function. ⊗ denotes the deconvolution operation. (x,y,z), θ and d_i respectively represent the Cartesian coordinates, orientation of observation, and the i-th depth, respectively. $i = 1, 2 \ldots. n$, and n is the number of different depths.

As shown in Fig. 16, the sum of the deconvoluted profiles includes erroneous profiles as well as the true profile. They are the results of the deconvolution with the PSFs at shallower depths than the true depths of the absorbing object. The effects of the erroneous profiles are suppressed in the second process of the developed technique. In the second process, we first reconstruct a cross-sectional image from the projection data or the sum of the deconvoluted profiles. This cross-sectional image from the deconvoluted profiles is better than that from the observed profiles, because the profiles at the deeper depths than the true depth were effectively erased by the deconvolution operation as shown in Fig. 16. In this improved cross-sectional image, we sample the absorption profiles at the same depths as those of the PSFs used in the first process. We call this profile an erasing template, $E(x,z\,|\,\theta,d_i)$. Then, we multiply these profiles as the templates to erase the unnecessary parts of the deconvoluted profiles. Figure 17 portrays this operation. Consequently, we emphasize the profiles only at

#205296 - $15.00 USD Received 23 Jan 2014; revised 6 Mar 2014; accepted 7 Mar 2014; published 1 Apr 2014

the true depths. Then they are summed up to make a new improved projection. This process can be written as

$$P_{new}(x,z\,|\,\theta)=\sum_{i=1}^{n}\sqrt{\left[\int A(x,y,z\,|\,\theta)dy\otimes PSF(x,z\,|\,d_i)\right]E(x,z\,|\,\theta,d_i)}, \qquad (4)$$

where P_{new}, A, PSF, and E respectively show the functions of new projection, blurred absorption distribution, point spread function, and the erasing template.

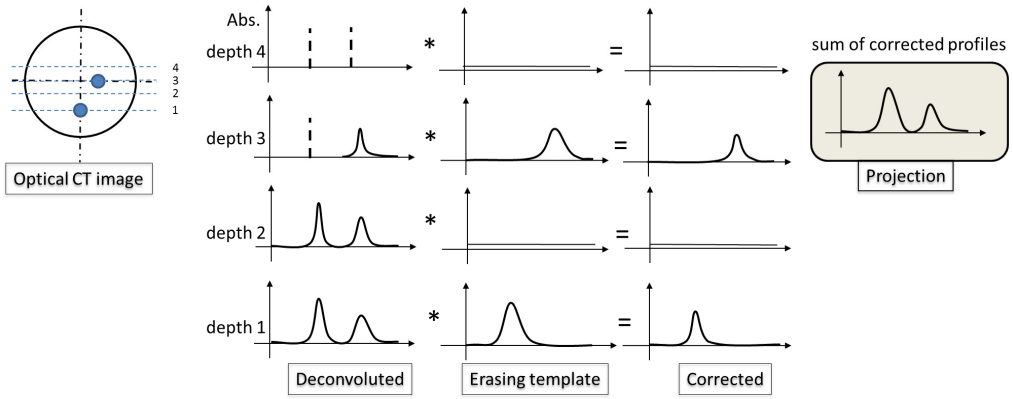

Fig. 17. Principle to suppress erroneous absorption distribution. Erroneous parts are suppressed by multiplying erasing templates obtained from the original cross-sectional image. New projection image is constructed as a sum of the corrected images. * denotes the multiplication operation.

Using the new projection image $P_{new}(x,z\,|\,\theta)$, we can reconstruct an improved 3D image with the filtered back-projection algorithm. This process can be repeated until a satisfactory result is obtained.

The effectiveness of the proposed technique was verified in computer simulation with the model shown in Fig. 18(a). The effect of scattering was suppressed by the proposed technique (number of different depths, n = 300) with a single step of the template erasure process as shown in Figs. 18(b)–18(d).

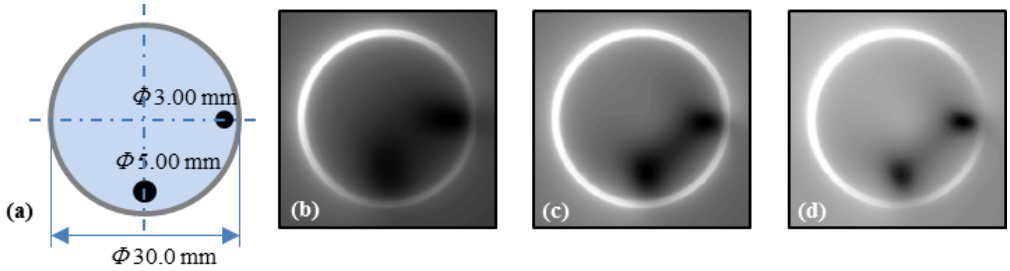

Fig. 18. Result of proposed technique in simulation: (a) simulation model (μ'_s = 1.00 /mm, μ_a = 0.00536 /mm), (b) cross-sectional image of two objects in scattering medium, (c) result from projection of Eq. (3), (d) result from projection of Eq. (4).

5. Experiment with phantom

The feasibility of the proposed technique, described in previous chapter, was examined in an experiment. Figure 19 presents a schematic of the experimental system to obtain transillumination images of a tissue-equivalent phantom. As scattering medium, Intralipid suspension (Fresenius Kabi AG) and black ink (INK-30-B; Pilot Corp.) were mixed with distilled water to produce a tissue-equivalent medium (μ'_s = 1.00 /mm, μ_a = 0.01 /mm). As an

#205296 - $15.00 USD Received 23 Jan 2014; revised 6 Mar 2014; accepted 7 Mar 2014; published 1 Apr 2014

absorbing structure, three black-painted objects as shown in Figs. 20(a) and 21(a) were used to simulate the high-absorbing structure in mouse body, such as kidneys and a spleen.

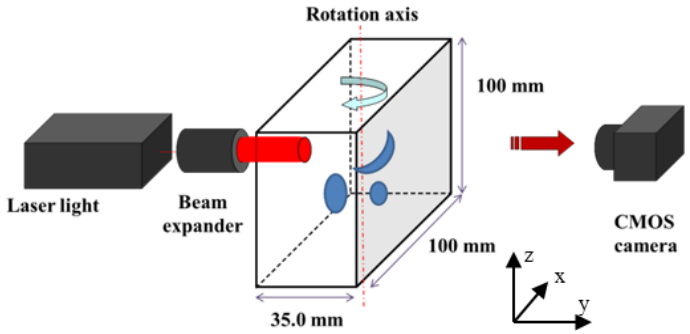

Fig. 19. Experimental setup with phantom.

The absorbing structure was placed at the center of an acrylic container (35.0 × 100 × 100 mm^3) filled with scattering medium. The phantom was irradiated with the NIR light from a laser (Ti:Sapphire, 850 nm wavelength) through a beam expander for homogeneous illumination. The image was captured using a cooled CMOS camera (C11440-10C; Hamamatsu Photonics K.K.) oriented toward the opposite face of the phantom to the light incident side. This recording was repeated while rotating the absorbing structure around the rotation axis using a mechanical rotation system.

Figures 20(a) and 21(a) respectively show the observed image of the absorbing structure in clear medium at 0 degree and 90 degree. Figures 20(b) and 21(b) show the observed image of the absorbing structure in scattering medium. Figures 20(c) and 21(c) show the result of the process described in chapter 4. The proposed technique was applied with the number of different depths n = 350 and with a single step of the template erasure process. The scattering effect was suppressed efficiently, and the absorbing objects were visualized.

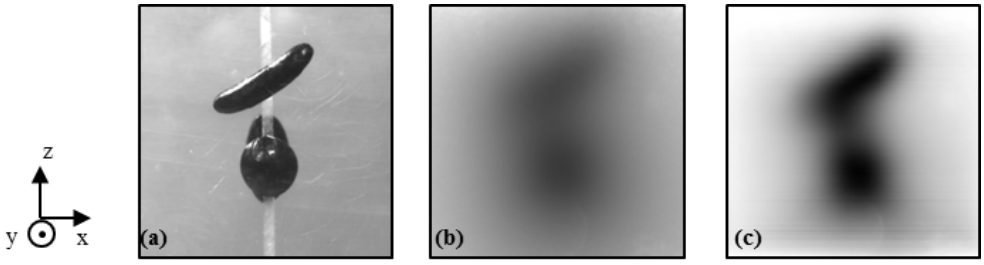

Fig. 20. Scattering suppression in transillumination imaging at 0-deg orientation: (a) observed image in clear medium, (b) observed image in scattering medium, (c) result using the proposed technique.

#205296 - $15.00 USD Received 23 Jan 2014; revised 6 Mar 2014; accepted 7 Mar 2014; published 1 Apr 2014

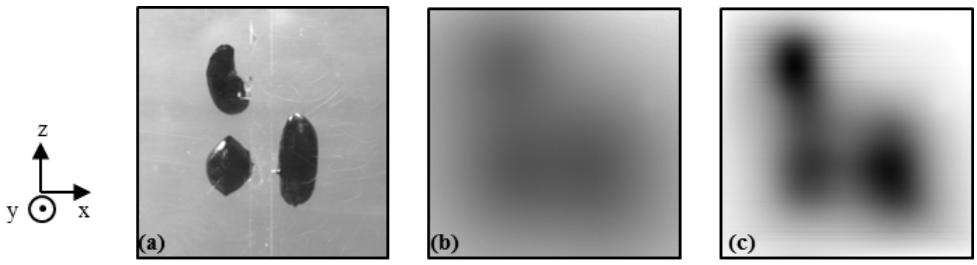

Fig. 21. Scattering suppression in transillumination imaging at 90-deg orientation: (a) observed image in clear medium, (b) observed image in scattering medium, (c) result using the proposed technique.

Figure 22 shows results with two-level thresholds, which are common in all the figures. The internal structure, which is hardly seen in Fig. 22(b), became visible by the proposed technique.

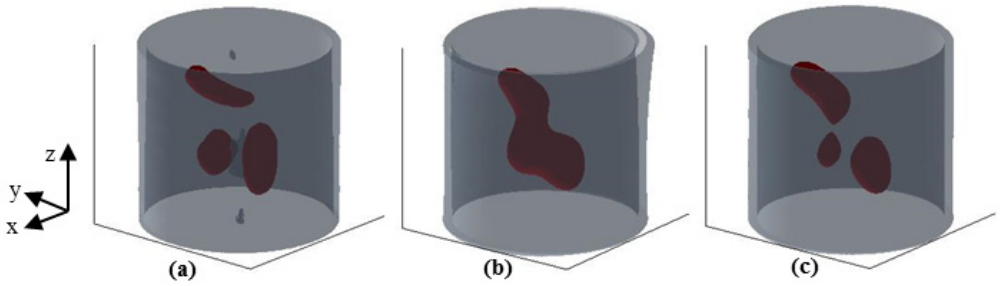

Fig. 22. 3D images reconstructed from transillumination images: (a) from observed image in clear medium, (b) from observed image in scattering medium, (c) result using the proposed technique.

6. 3D imaging of animal body

To examine the applicability of the proposed technique to a living animal body, experiments were conducted with a mouse. Figure 23 shows the experimental setup. A female mouse Slc:ICR (20 weeks old) was anesthetized by the intraperitoneal injection of pentobarbital (Nembutal). The mouse was held in a cylindrical holder made of transparent acrylic resin. Laser light (Ti:Sapphire, 850 nm wavelength) was illuminated from one side of the holder. Then the image was recorded using a CMOS camera (C11440-10C; Hamamatsu Photonics K.K.) from another side.

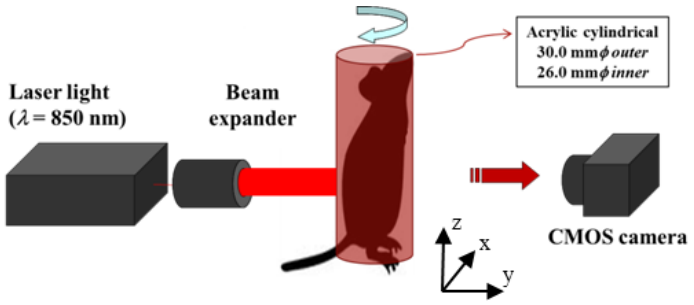

Fig. 23. Setup for experiment with living animal.

#205296 - $15.00 USD Received 23 Jan 2014; revised 6 Mar 2014; accepted 7 Mar 2014; published 1 Apr 2014

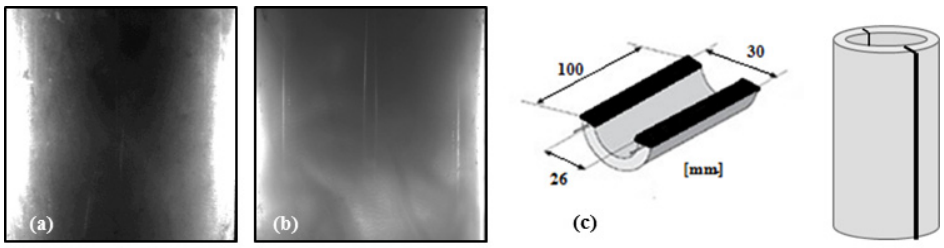

Fig. 24. Suppression of body-surface illumination caused by light-guide effect in cylindrical container: (a) without light trap, (b) with light trap, (c) light trap structure.

Special caution had to be taken to obtain transillumination images. Figure 24(a) presents an example of the transillumination image obtained with the experimental setup shown in Fig. 23. The surface of the mouse was lighted up, and the internal structure could hardly be seen because of the light guide effect of the acrylic cylinder. The incident light was guided through the cylindrical acrylic wall, subsequently illuminating a wide area of the body-surface of the mouse. To prevent this phenomenon, we cut the cylinder half and installed light traps in the cylinder wall. Figure 24(c) presents the light trap structure. Figure 24(b) shows the transillumination image obtained in the same experimental setup (Fig. 23) using the cylindrical mouse holder with light traps. By suppressing body-surface scattering, the internal structure came out in the image. The recording of a transillumination image was repeated while rotating the holder around the rotation axis shown in Fig. 23 using a mechanical rotation system. Figure 25 shows typical transillumination images obtained before and after the scattering suppression of the proposed technique. The internal light-absorbing structure became visible when using the proposed technique. From these transillumination images, the cross-sectional images were reconstructed using the proposed technique described in chapter 4. The proposed technique was applied with the number of different depths n = 350 and with a single step of the template erasure process.

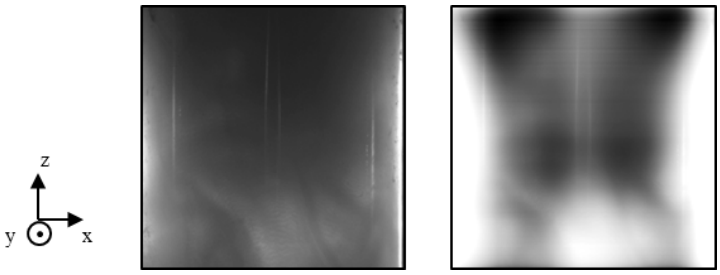

Fig. 25. Transillumination images of mouse abdomen: (a) observed image, (b) deconvoluted image with PSF (μ'_s = 1.5 /mm, μ_a = 0.02 /mm).

These cross-sectional images were piled up vertically and a 3D image was constructed. Figure 26 presents results with three-level thresholds. Common thresholds were used for Figs. 26(a) and 26(b). The internal structure hardly seen in Fig. 26(a) became visible using the proposed technique. The high-absorption organs such as kidneys and the bottom parts of the liver were identified.

#205296 - $15.00 USD Received 23 Jan 2014; revised 6 Mar 2014; accepted 7 Mar 2014; published 1 Apr 2014

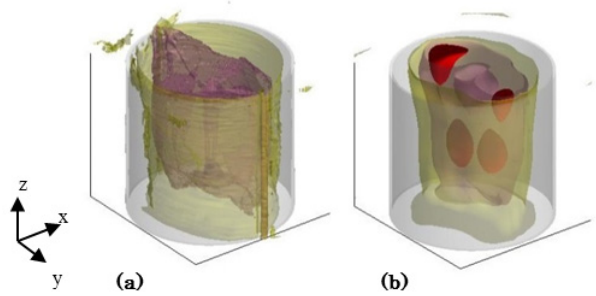

Fig. 26. 3D images reconstructed from transillumination images of mouse: (a) from observed images, (b) result using the proposed technique.

This experimental study verified the feasibility of the practical 3D imaging of the internal light-absorbing structure of a small animal.

7. Conclusions

With a view toward the imaging of the internal absorbing structure in an animal body, a new technique was developed to reconstruct the three-dimensional structure from transillumination images. To suppress the blurring effect of scattering in biological tissues, we applied the deconvolution method with a point spread function. Through theoretical and experimental study, we confirmed the applicability of the PSF for the light source to the transillumination images of the light-absorbing structure. We also confirmed the effectiveness of this technique in the experiment with a tissue-equivalent phantom.

The PSF is depth-dependent, and the technique explained above was applicable only for an object with known internal structure. To expand the applicability of this technique, we devised new algorithms. An observed transillumination image is deconvoluted with the PSFs of different depths. Then the deconvoluted images are summed up to produce a new image that serves as a projection image in cross-sectional reconstruction. The projection image contains the projection of the true absorption distribution and the incompletely deconvoluted projection as well. To suppress the effect of this erroneous projection, we devised an erasing process. A cross-sectional image is reconstructed from the projection images obtained from many orientations. It is used as a template to erase the erroneous distribution in the cross-section. After the application of this erasing process, a new improved projection image is formed in which the effect of the erroneous distribution is suppressed effectively.

The feasibility of the proposed technique was examined in a computer simulation and an experiment with a model phantom. The results demonstrated the effectiveness of the proposed technique. Finally, the applicability of the proposed technique to an living animal was examined. An anesthetized mouse was fixed in a transparent cylinder. We devised a light trap in the cylinder to produce a transillumination image of good quality. Using the proposed technique, the 3D structure of the mouse abdomen was reconstructed. High-absorbing organs such as the kidneys and parts of livers became visible.

Results of this study suggest that we can expect a new optical CT having different features from those of currently available techniques such as conventional diffuse optical tomography (DOT) techniques. This simple system can provide a cross-sectional image and reconstruct the 3D structure of internal organ in the mouse body. It can provide a useful and safe tool for the functional imaging of internal organs of experimental animals and for optical CT imaging of the near-surface structure of the human body.

Acknowledgments

A part of this research was supported by a Grant-in-Aid for Scientific Research from the Japan Society for the Promotion of Science. The animal experiment in this study was conducted in accordance with the guidelines [38] and with the approval of the review committee for animal experiments at Hokkaido University.

#205296 - $15.00 USD Received 23 Jan 2014; revised 6 Mar 2014; accepted 7 Mar 2014; published 1 Apr 2014